CHEMISTRY OF MATERIALS

Article

pubs.acs.org/cm

Invar-like Behavior of Antiperovskite $Mn_{3+x}Ni_{1-x}N$ Compounds

Sihao Deng,[†] Ying Sun,*[,†] Hui Wu,[‡,∥] Qingzhen Huang,[‡] Jun Yan,[†] Kewen Shi,[†] Muhammad Imran Malik,[†] Huiqing Lu,[†] Lei Wang,[†] Rongjin Huang,[§] Laifeng Li,[§] and Cong Wang*[,†]

[†]Center for Condensed Matter and Materials Physics, Department of Physics, and Key Laboratory of Micro-nano Measurement, Manipulation and Physics (Ministry of Education), Beihang University, Beijing 100191, People's Republic of China

[‡]NIST Center for Neutron Research, National Institute of Standards and Technology, Gaithersburg, Maryland 20899-6102, United States

[§]Key Laboratory of Cryogenics, Technical Institute of Physics and Chemistry, Chinese Academy of Sciences, Beijing 100190, People's Republic of China

[∥]Department of Materials Science and Engineering, University of Maryland, College Park, Maryland 20742-2115, United States

Supporting Information

ABSTRACT: The antiperovskite $Mn_{3+x}Ni_{1-x}N$ compounds have been synthesized and characterized by a variety of experimental techniques. After Mn doping at the Ni site, both ferromagnetic characteristics and an Invar-like effect were observed in the antiferromagnetic host material. The observed Invar-like behavior was assumed to be related to the characteristic magnetic structure induced by the doping. Neutron diffraction results prove that the Mn doping stabilizes the special Γ^{5g} antiferromagnetic phase with strong spin−lattice coupling that can be tuned to achieve Invar-like behavior. The magnetovolume effect (MVE) and significant correlation between spin and lattice were confirmed for the Γ^{5g} magnetic phase by the first-principles calculations. Moreover, Mn 3d electrons were revealed to be the key factor for the MVE from the calculations. Our study presents a new mechanism for precisely controlling the zero thermal expansion of a single compound by achieving the special Γ^{5g} magnetic phase of Mn atoms.

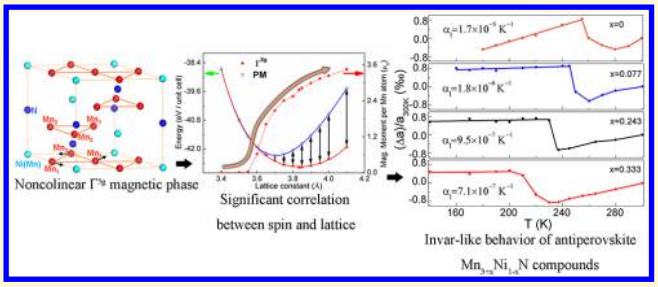

INTRODUCTION

Most of the materials show positive thermal expansion (PTE); the exceptions are fascinating. Materials with near-zero thermal expansion (NZTE) or negative thermal expansion (NTE) have been the subject of fundamental studies and are highly desirable for many modern technological applications.[1−5] However, the mechanism of abnormal thermal expansion (ATE), which contains NZTE, ZTE, and NTE, remains unclear. Tremendous effort has been devoted to finding new materials and modifying the ATE behavior. A mechanism related to the soft-phonon modes in the framework structures has been proposed to explain the NTE in ZrW_2O_8[2,6] and ScF_3.[7] Interestingly, some NTE and ZTE materials exhibit a strong coupling between ATE and other physical properties, such as a change in the electronic valence state in $LaCu_3Fe_4O_{12}$,[8] $BiNiO_3$,[9] and YbGaGe,[1] or ferroelectricity weakening in $PbTiO_3$−$BiFeO_3$ perovskite.[10] Also, a large amount of ATE materials accompanied by magnetic ordering has been extensively studied such as NTE in $La(Fe,Si,Co)_{13}$[11] and $Ca_2Ru_{1-x}Cr_xO_4$,[12] or NZTE in FeNi Invar alloys[13] and $SrRuO_3$.[14] In particular, the Invar effect was suggested to be related to magnetism. However, a clear explanation about the origin of NZTE[13] is still lacking. Therefore, the discovery of new Invar-like materials will be essential for clarifying the mechanism of Invar behavior.[14−20]

Recently, the Invar-like effect, showing NZTE or ZTE, has been observed with magnetovolumic instabilities in both ferromagnetic (FM) and antiferromagnetic (AFM) ground-state compounds.[15,16] It was reported that the Invar-like effect occurred in $CaRu_{0.85}Fe_{0.15}O_3$ below T_C, signifying that the anomalous volume expansion is due to the MVE caused by the occurrence of ferromagnetism.[15] On the other hand, for the NpFeAsO with an AFM ground state, it was also found that the magnetic transition was accompanied by a large expansion of the unit cell volume below T_N followed by an Invar behavior below 20 K.[16]

Interestingly, besides the regular FeNi Invar alloys,[13] anisotropic thermal expansion and cooperative Invar and anti-Invar effects were observed in Mn alloys, such as $Mn_{87}Pd_{13}$,[17] $Mn_{85}Zn_{15}$,[18] and $Mn_{88}Ni_{12}$.[19] For $Mn_{88}Ni_{12}$, the two-state model (in Mn) with collinear AFM structure was concluded to describe the cooperative Invar and anti-Invar effects. To achieve isotropic thermal expansion in Mn alloys, further efforts are still needed by tuning the crucial magnetic properties. Notably, the Invar-like effect within a noncolinear AFM structure was rarely observed. As for the noncolinear AFM ground-state com-

Received: December 21, 2014
Revised: March 1, 2015
Published: March 3, 2015

DOI: 10.1021/cm504702m
Chem. Mater. 2015, 27, 2495−2501

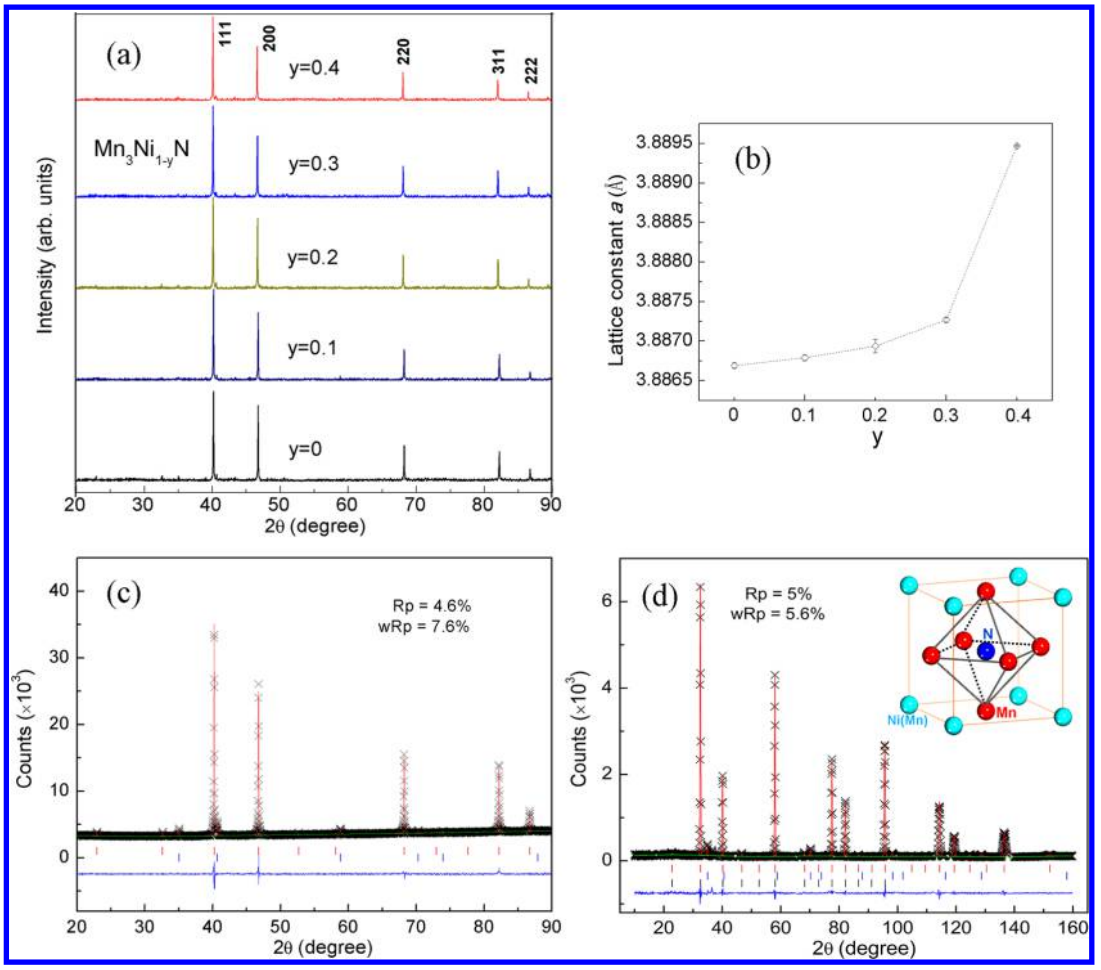

Figure 1. Room-temperature (a) XRD patterns and (b) composition (y) dependence of the lattice constant from refined results with the nominal $Mn_3Ni_{1-y}N$ composition (y = 0, 0.1, 0.2, 0.3, and 0.4). Rietveld refinement analysis of both (c) XRD and (d) NPD patterns for the nominal composition $Mn_3Ni_{0.6}N$ at room temperature. The crosses show the experimental intensities (I_{obs}); the top solid line shows the calculated intensities (I_{calc}), and the bottom solid line is the difference between the observed and calculated intensities ($I_{obs} - I_{calc}$). The vertical lines indicate the angular positions of the nuclear (top row), MnO (second row), and magnetic (third row) Bragg reflections.

pounds, many researchers have focused on the isotropic NTE behaviors near the magnetic transition temperature in manganese-based antiperovskite compounds Mn_3XN (X = Zn, Cu, Ni, etc.), which are also accompanied by a variety of fascinating physical properties caused by strong correlation among lattice, spin, and charge.[20−26] It is also important to mention that the isotropic NTE behavior in pure Mn_3XN could be extended to a wider temperature window by substitution or doping at the X site,[23,26] and this provides a useful method for controlling the thermal expansion behaviors near the magnetic transition temperature. However, there have not been many studies about the low thermal expansion behaviors below T_N,[24−26] even though isotropic ZTE behavior may be possible by doping in these materials.[20]

Neutron diffraction revealed that noncolinear Γ^{5g} AFM spin structure was a key ingredient for the large MVE in antiperovskite systems with itinerant electron characteristic.[27] Also, theoretical studies confirmed that Mn_3XN compounds experience a volume variation because of the difference in the equilibrium lattice constants for Γ^{5g} AFM and paramagnetic (PM) phases.[28,29] Moreover, using neutron powder diffraction (NPD), we have discussed the origin of the isotropic ZTE of the cubic antiperovskite compounds $Mn_3(Zn/Ag/Ge)_xN$ and tuning of the special Γ^{5g} AFM spin structure and related ZTE behavior.[20] It is worth noting that Mn_3NiN exhibits a magnetic structure with a combination of Γ^{5g} and Γ^{4g} symmetries[25] and displays low thermal expansion properties below T_N.[26] To validate the relationship between magnetic structure and their thermal expansion behavior and control the resultant properties, we prepared $Mn_{3+x}Ni_{1-x}N$ compounds with Mn doping at the Ni site. Using NPD and first-principles calculations, we discussed the mechanism of the NTE and Invar-like behavior observed in this material.

EXPERIMENTAL AND COMPUTATIONAL SECTION

Synthesis. Polycrystalline samples of the nominal composition $Mn_3Ni_{1-y}N$ (y = 0, 0.1, 0.2, 0.3, or 0.4) were prepared by solid-state reaction using Mn_2N, which was synthesized by sintering Mn powder (4 N) in nitrogen gas, and Ni (3 N) as the starting materials. The detailed preparation is described in the Supporting Information.[20,21]

Measurements. X-ray diffraction (XRD) patterns at room temperature were obtained from an X'Pert PRO powder diffractometer using Cu Kα radiation. To determine the thermal expansion properties, variable-temperature XRD ranging from 140 to 300 K was performed using in situ powder XRD equipment (BRUKER D8-discover diffractometer with Cu Kα radiation). Crystal structures were determined by the Rietveld refinement method with the General Structure Analysis System (GSAS).[30] The temperature dependence of magnetization was measured between 10 and 350 K under a 0.5 kOe

DOI: 10.1021/cm504702m
Chem. Mater. 2015, 27, 2495−2501

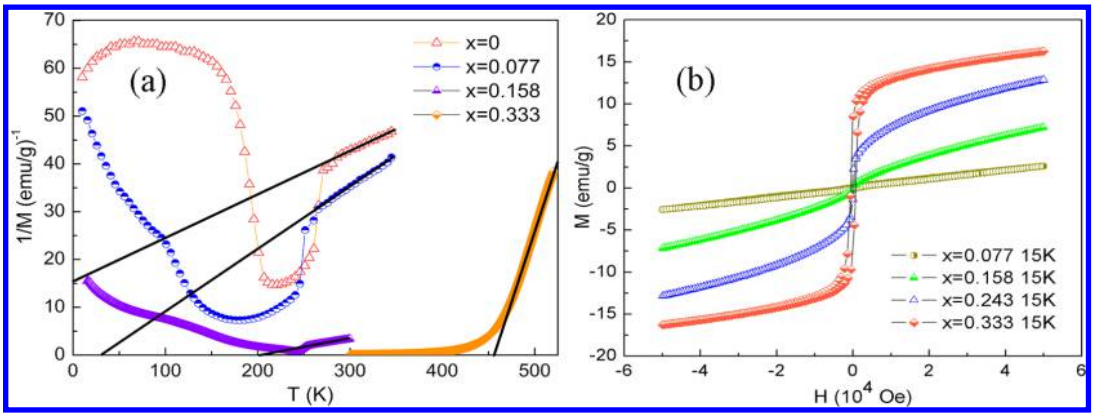

Figure 2. (a) Temperature dependence of inverse magnetization (ZFC) of $Mn_{3+x}Ni_{1-x}N$ compounds. Solid lines correspond to a linear fitting. (b) Isothermal magnetization of the $Mn_{3+x}Ni_{1-x}N$ compounds at 15 K.

magnetic field using a Physical Property Measurement System (PPMS). The measurements were conducted under both zero-field-cooling (ZFC) and field-cooling (FC) conditions, and the isothermal magnetization curve was recorded between −50 and 50 kOe. In addition, the temperature dependence of magnetization between 300 and 520 K was also measured by a vibration sample magnetometer (VSM).

Neutron powder diffraction (NPD) data were collected using the BT-1 high-resolution neutron powder diffractometer at the NIST Center for Neutron Research (NCNR). A Cu(311) monochromator with a wavelength of 1.5403 Å was used. To explain the magnetic transitions, neutron diffraction data were collected at various temperatures of interest in the range of 5−300 K. The GSAS was used for Rietveld refinement with scattering lengths of -0.375×10^{-12}, 1.030×10^{-12}, and 0.936×10^{-12} cm for Mn, Ni, and N, respectively. The antiperovskite crystal and magnetic structures of Mn_3NiN are shown in the inset of Figure 1d.[31] Ni [at 1a(000)] atoms are on the corners of the cubic lattice; Mn atoms are at face centers, and the N atom is at body center, forming a Mn_6N octahedron.

Computational Description. We performed the first principle study using the projector augmented-wave (PAW) method initially proposed by Blöchl.[32] For fully unconstrained noncollinear magnetic structures, we used the execution of Kresse and Joubert in VASP code[33] within the Perdew−Burke−Ernzerhof (PBE) generalized gradient approximation.[28,29,34] The cutoff energy of 500 eV and Gamma-centered k points with a 3 × 3 × 3 grid were used. The Γ^{5g} magnetic structure with the spins on the (111) plane was employed. The nonmagnetic (NM) supercell with zero total magnetic moment was adopted and mimicked a high-temperature paramagnetic phase. To study the MVE, a $Mn_{42}Ni_6N_8$ supercell, corresponding to the composition of $Mn_{3.25}Ni_{0.75}N$, was used in our calculations. On the basis of the supercell that contains 2 × 2 × 2 chemical unit cells of Mn_3NiN, two Ni atoms were substituted with Mn with three different options to obtain the stabilized system.

RESULTS AND DISCUSSION

Figure 1a shows the room-temperature powder XRD patterns of nominal composition $Mn_3Ni_{1-y}N$ (y = 0, 0.1, 0.2, 0.3, or 0.4), indicating that all the samples are cubic perovskite structure (space group $Pm\bar{3}m$). The y-dependent values of lattice constants are plotted in Figure 1b, which were obtained from the standard Rietveld refinement. For example, Figure 1c shows a representative XRD pattern fit of the nominal composition $Mn_3Ni_{0.6}N$, and a small amount of MnO could be found. The Rietveld fits on other XRD patterns are shown in Figure S1 of the Supporting Information. Figure 1b shows that the lattice constant gradually increases with decreasing Ni content or increasing Ni vacancy, which shows an abnormal phenomenon. In principle, the shrinkage of the lattice should be observed when the Ni vacancies increase. The refined compositions y in $Mn_3Ni_{1-y}N$ are determined to be 0.02, 0, 0, 0, and 0.01 for nominal compositions of y = 0, 0.1, 0.2, 0.3, and 0.4, respectively. This confirms that the Ni atom sites on the corners of the cube are almost fully occupied. The further refinement showed that it is Mn that occupies the Ni site and forms $Mn_3Ni(Mn)_{1-y}N$. Therefore, the increase in the lattice constant with an increasing y can be explained by the smaller Ni substituted with the larger Mn. In the case, the formula would be $Mn_{3+x}Ni_{1-x}N$, and the relationship between x and y is

$$(3 + x): (1 - x) = 3:(1 - y) \quad (1)$$

The x values (Mn doping concentrations) are 0.077, 0.158, 0.243, and 0.333 for y = 0.1, 0.2, 0.3, and 0.4, corresponding to $Mn_{3.077}Ni_{0.923}N$, $Mn_{3.158}Ni_{0.842}N$, $Mn_{3.243}Ni_{0.757}N$, and $Mn_{3.333}Ni_{0.667}N$ compositions, respectively. To further verify the Mn doping of $Mn_{3+x}Ni_{1-x}N$, Rietveld analysis including occupancy refinement was performed using NPD data. Figure 1d displays the NPD patterns of the nominal $Mn_3Ni_{0.6}N$ composition at room temperature. A small amount of MnO could be found in Figure 1d. The diffraction peaks from the Al sample holder are excluded from the analysis. The NPD patterns could be fit well by a structural model of cubic symmetry shown in the inset of Figure 1d. The magnetic properties with the variation of temperature will be discussed below. The refined composition is determined to be $Mn_{3.338}Ni_{0.651}N$, which is almost the same as the calculated formula $Mn_{3.333}Ni_{0.667}N$ from eq 1, indicating that Mn-doped compounds of $Mn_{3+x}Ni_{1-x}N$ are in fact synthesized instead of compounds with Ni vacancies. Subsequently, we will use these $Mn_{3+x}Ni_{1-x}N$ compositions with Mn doping at the Ni site unless explicitly indicated otherwise.

The magnetic properties of the $Mn_{3+x}Ni_{1-x}N$ antiperovskite materials are shown in detail in Figure 2 and Figure S2 of the Supporting Information. As shown in Figure S2 of the Supporting Information, with increasing x the peak of magnetization $M(T)$ increases by approximately 200 times from 0.07 (x = 0) to 14.8 emu/g (x = 0.333), revealing that Mn doping induces increasing ferromagnetism in the AFM metallic host material Mn_3NiN.[25,31] The Curie−Weiss law is used to further investigate the magnetic properties in these compounds as shown in Figure 2a. It can be seen that the Θ_W (−164, 32, 204, and 455 K at x = 0, 0.077, 0.158, and 0.333, respectively) with increasing x changes from negative to positive, indicating that the AFM interactions quickly develop into FM interactions with increasing Mn concentrations. In addition, the FM

DOI: 10.1021/cm504702m
Chem. Mater. 2015, 27, 2495−2501

interactions are also confirmed by the isothermal magnetization $M(H)$ measurements presented in Figure 2b. It is clear that the $M - H$ curve at 15 K is almost linear for $x = 0.077$, while for increasing values of x, it exhibits more FM characteristic, suggesting the FM interactions were induced by the Mn doping. This is in agreement with the previous discussion. However, when x is increased to 0.333, the magnetization does not tend to saturation even though the field is increased to 50 kOe and the magnetization M is above 16 emu/g, indicating the possible coexistence of FM and AFM ordering phases in this composition.[35]

Linear thermal expansion $\Delta a/a_{300\ K}$ of $Mn_{3+x}Ni_{1-x}N$ is shown in Figure 3. It is worth mentioning that the anomalies in

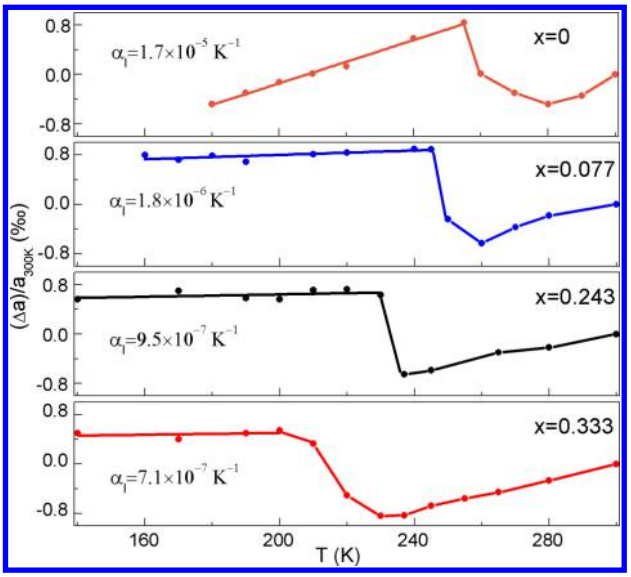

Figure 3. Linear thermal expansion ($\Delta a/a_{300\ K}$; $\Delta a = a - a_{300\ K}$) for $Mn_{3+x}Ni_{1-x}N$ compounds (x = 0, 0.077, 0.243, and 0.333). $a_{300\ K}$ represents the lattice constant at 300 K for these compounds.

$\Delta a/a_{300\ K}$ appear at the magnetic transition temperature, which decreases with increasing x for all compounds. Another exceptional characteristic is that a ZTE behavior exists below the magnetic transition temperature in some of the $Mn_{3+x}Ni_{1-x}N$ compounds. With increasing x, the coefficient of linear thermal expansion α_l obtained from the X-ray diffraction data decreases from 1.7×10^{-5} K^{-1} (180−255 K; $x = 0$) to 1.8×10^{-6} K^{-1} (160−245 K; $x = 0.077$). In particular, α_l is in the range of 10^{-7} K^{-1} for x values of 0.243 (140−230 K) and 0.333 (140−200 K), which is generally considered ZTE.[20] A similar ATE-accompanied Invar-like effect below the first-order transition temperature was also found in NpFeAsO and $CaRu_{0.85}Fe_{0.15}O_3$.[15,16]

To clarify the mechanism of the ATE behaviors, NPD studies at variable temperatures were performed. Figure 4a shows the NPD pattern of $Mn_{3.333}Ni_{0.667}N$ at 5 K. The NPD pattern could be fit well with a structural model of cubic symmetry shown in the inset of Figure 1d, and a supperlattice magnetic model is shown in Figure 4b. The refined AFM moment for Mn is 2.16(2) μ_B, and the FM components from Mn_4 are 5.2(2) μ_B (~1.73 μ_B/atom at the corner). Figure 4c shows the profile difference ($I_{obs} - I_{calc}$) of nuclear fitting only (black) for $Mn_{3.333}Ni_{0.667}N$ at 5 K, where the significant profile difference indicates the presence of magnetic peaks. However, if we use the Γ^{5g} magnetic model to fit the magnetic peaks in the NPD pattern of $Mn_{3.333}Ni_{0.667}N$, the refinement is still unreasonable because large discrepancies remain in the profile difference ($I_{obs} - I_{calc}$) of nuclear and Γ^{5g} AFM fitting (blue solid line). We therefore use the magnetic model shown in Figure 4b. The refinement converged rapidly, and the refined results are reasonable, as indicated by the small profile difference shown in the top line of Figure 4c. For Mn_3NiN, it has been investigated previously, with a combination of Γ^{5g} and Γ^{4g} AFM phase structures below $T_N \sim 250$.[25,31] However, our NPD study indicates that the AFM phase becomes single Γ^{5g} symmetry in the $Mn_{3.333}Ni_{0.667}N$ compound at 5 K, suggesting that we could stabilize the Γ^{5g} AFM phase while eliminating the Γ^{4g} magnetic phase by increasing the level of Mn doping at the Ni site. On the other hand, the magnetic moment of Mn_4 along the c-axis suggests an FM behavior in $Mn_{3.333}Ni_{0.667}N$.

In $Mn_{3.333}Ni_{0.667}N$, the face-centered Mn atoms with Mn_6N octahedra show Γ^{5g} AFM spin structure, whereas the Mn atoms at the cubic corner have FM components. We suggest that the ATE behavior of $Mn_{3.333}Ni_{0.667}N$ is associated with Γ^{5g} AFM spin structure of Mn atoms at face-centered sites because of the following considerations. (1) As reported previously, local structural information confirmed that the local lattice distortion described by the alternating rotation of the Mn_6N octahedra around the c-axis is considered to be a good indicator for studying the MVE in antiperovskite compounds.[36] (2) The ZTE behavior that is controlled by Γ^{5g} AFM spin structure of Mn atoms was verified in antiperovskite compounds $Mn_3(Zn/Ag/Ge)_xN$.[20] (3) We also confirmed that the MVE in Mn_3NiN originates from coupling of the Γ^{5g} AFM spin structure with the cubic crystal structure in the previous NPD study.[25] (4) For Mn_4N, which has the same crystal structure as $Mn_{3+x}Ni_{1-x}N$, ferrimagnetic ordering that originated from the two non-equivalent sites at the corner and the face-centered Mn atoms has been found.[37] However, the MVE was not observed in a Mn_4N compound even though the Mn atoms at the corner showed a magnetic ordering similar to that of $Mn_{3+x}Ni_{1-x}N$.[37,38] Therefore, the face-centered Mn atoms are recognized as the key factor in the ATE phenomenon in the following discussion.

As shown in the NTE region of Figure 4d, the Γ^{5g} ordered moment of Mn suddenly drops rapidly when the compound displays NTE behavior. This abrupt increase in the volume in the same temperature range indicates a close correlation between the anomalous volume variation and the magnetic ordering, confirming that the lattice is coupled with Mn magnetic ordering. Figure S3 of the Supporting Information gives more details about the correlation between thermal expansion behaviors and intensities of the magnetic peak. In general, the NTE or ZTE behavior in antiperovskite materials is recognized as a result of a competition between the contraction of the lattice upon heating due to the magnetic ordering and normal thermal expansion.[20,39] The existence of the ATE allows a quantitative evaluation of the magnetic coupling to the lattice for the Γ^{5g} phase.[20] Moreover, the effect of the Γ^{5g} phase connects with not only the magnitude of the magnetic moment but also the degree of magnetic moment variation with temperature variation, i.e., $\Delta a(T)/\Delta T(T) = [\Delta a(T)/\Delta M(T)]$-$[\Delta M(T)/\Delta T(T)]$. Figure 4d shows $\Delta M/\Delta T$ is almost steady in ZTE while it is in an acute form in the NTE region, indicating that the ZTE behavior is considered particularly noteworthy for studying spin−lattice coupling. In addition, the different $\Delta M/\Delta T$ may be responsible for the different ATE (NTE and Invar-like) behaviors in antiperovskite compounds

DOI: 10.1021/cm504702m
Chem. Mater. 2015, 27, 2495−2501

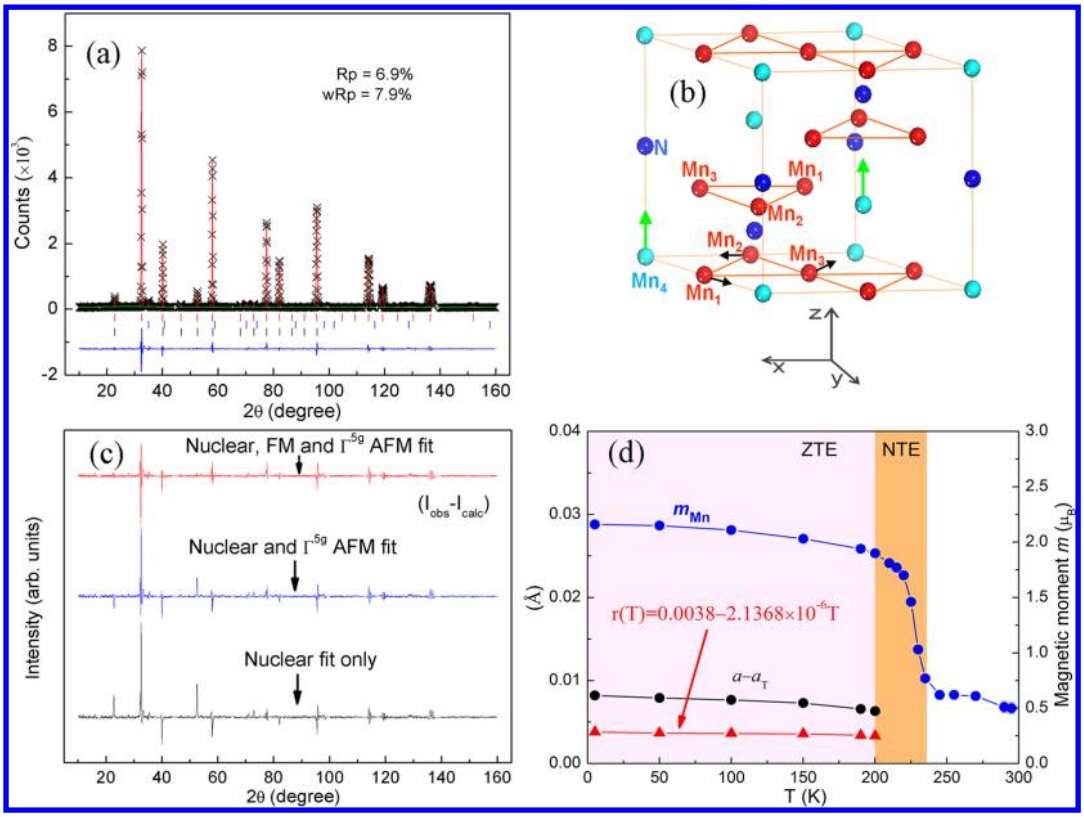

Figure 4. (a) Neutron powder diffraction patterns of $Mn_{3.333}Ni_{0.667}N$ at 5 K. The details of refinement are given in Figure 1d. (b) Magnetic structure of $Mn_{3.333}Ni_{0.667}N$, corresponding to rhombohedral ($R\bar{3}$) magnetic symmetry (Γ^{5g}) for Mn (Mn_1, Mn_2, and Mn_3) atoms. (c) The top solid line shows the profile difference ($I_{obs} - I_{calc}$) generated by nuclear, FM, and Γ^{5g} AFM fits at 5 K. The second line shows $I_{obs} - I_{calc}$ generated by nuclear and Γ^{5g} AFM fitting at 5 K. The bottom line shows $I_{obs} - I_{calc}$ generated by nuclear fitting only at 5 K. (d) Temperature dependence of the lattice variation $a(T) - a_T(T)$, ordered magnetic moments (m_{Mn}) of the Γ^{5g} AFM structure, and $r(T)$ for $Mn_{3.333}Ni_{0.667}N$.

with temperature. The Invar-like effect seems to appear when the MVE approaches saturation below the magnetic transition temperature.[15]

To further study spin−lattice coupling of Mn-based antiperovskite materials in the Invar-like behavior region, we assume that $\alpha_T(T) = \alpha_{PTE}(T)$, where $\alpha_T(T)$ and $\alpha_{PTE}(T)$ are defined as the coefficient of the usual thermal expansion contributed by the lattice anharmonic vibration in the Invar-like behavior and PTE region, respectively. Then we can get $a_T(T)$ from the fitting curve of PTE constants using a cubic function[20] (shown in eq 1 of the Supporting Information) in which $a_T(T)$ represents the lattice constant contributed by the lattice anharmonic vibration in the Invar-like behavior region. Marking $a(T)$ as the observed lattice constant, we take the difference $\Delta a_m(T) = a(T) - a_T(T)$ to isolate the effect of the NTE. Figure 4d shows the $\Delta a_m(T)$ of $Mn_{3.333}Ni_{0.667}N$ in the Invar-like behavior region decreases modestly with an increasing temperature, which is in agreement with the decreasing trend of the ordered Mn moment. Moreover, the ratio $r(T) = \Delta a_m(T)/M(T)$ is defined as the value of the NTE effect connected with the magnitude of the ordered moment, where $M(T)$ is the magnetic moment of the Mn atom. For $Mn_{3.333}Ni_{0.667}N$, the ratio $r(T)$, which has an extremely low coefficient value of 10^{-6} as a linear function, is approximately independent of T in the Invar-like behavior region, indicating a strong spin−lattice coupling phenomenon in this sample. This model has been used in Mn_3Zn_xN and $Mn_3Zn_{0.41}Ag_{0.41}N$ compounds with spin−lattice coupling.[20] On the other hand, it is significant that the Γ^{4g} ordered moment of the Mn atom in Mn_3NiN[25] was almost constant in the low-thermal expansion region. This contribution may weaken the MVE, thus destroying the Invar-like behavior of the host Mn_3NiN.

It has been revealed that the noncollinear Γ^{5g} magnetic structure plays a crucial role in the ATE behavior of Mn-based antiperovskite compounds because of the special contribution to the MVE. To understand the mechanism of the MVE, Figure 5 illustrates the characteristics of Γ^{5g} AFM and PM phases of $Mn_{3.25}Ni_{0.75}N$, the composition of which is close to those of

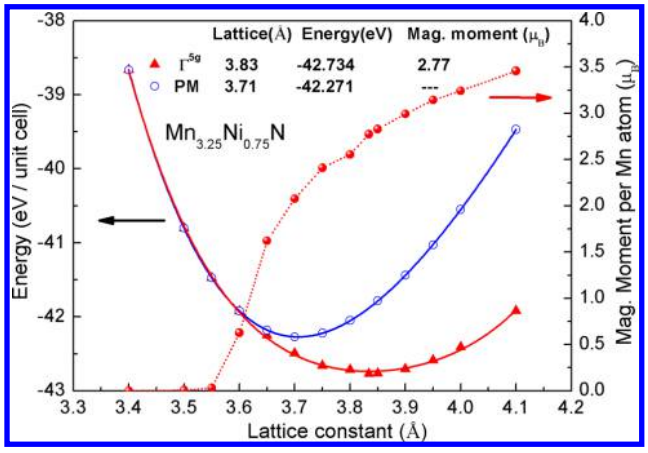

Figure 5. Energy and local magnetic moment of Mn atoms as a function of the lattice constant for Γ^{5g} AFM and PM phases of the $Mn_{3.25}Ni_{0.75}N$ sample.

DOI: 10.1021/cm504702m
Chem. Mater. 2015, 27, 2495−2501

$Mn_{3.243}Ni_{0.757}N$ and $Mn_{3.333}Ni_{0.667}N$ compounds that display the ZTE behaviors. Figure 5 shows that the calculated equilibrium lattice constant of the Γ^{5g} magnetic structure for $Mn_{3.25}Ni_{0.75}N$ is 3.83 Å, which is comparable to the experimental value of 3.887 Å ($Mn_{3.243}Ni_{0.757}N$) at room temperature. The averaged local magnetic moment of Mn (Γ^{5g} magnetic structure) is predicted to be 2.77 μ_B/Mn atom, which is close to the experimentally observed value of 2.16(2) μ_B/atom in $Mn_{3.333}Ni_{0.667}N$ and the calculated value of 2.63 μ_B/atom.[28] The magnetic moment of Mn_4 on the corners of the cube is 3.1 μ_B/Mn atom, which is smaller than the experimental result of 5.2(2) μ_B/Mn atom (~1.73 μ_B/atom at the corner) in $Mn_{3.333}Ni_{0.667}N$. However, it does not affect the analysis of MVE. Moreover, the magnetic structure is the same as the NPD refined result. On the other hand, the total energy of the Γ^{5g} magnetic structure is 0.463 eV/f.u (f.u. is the abbreviation of formula unit). lower than that of the PM state at their optimal lattices. The equilibrium lattice constant of the PM state is 3.71 Å, which corresponds to a lattice contraction of 0.12 Å ($\Delta a/a$ = 0.031) from the AFM to PM state. This qualitatively agrees with the observed Γ^{5g} → PM first-order phase transition of $Mn_{3.243}Ni_{0.757}N$ and $Mn_{3.333}Ni_{0.667}N$ with a $\Delta a/a$ of 0.0013. The calculated value of $\Delta a/a$ is a slightly greater than the observed values. However, it does not affect the qualitative analysis of MVE because such disagreement always exists in the current density functional theory calculation.[29,40] Although the cause of this discrepancy is not known at present, we presume that it is due to the neglected local environment effects[40] and the contribution of temperature[29] within the PM model.

From the NPD results, the spin−lattice coupling was found with variation of temperature. We present the significant correlation between spin and lattice theoretically to further address and validate this phenomenon. Figure 5 shows the Mn local magnetic moment in the Γ^{5g} magnetic structure is extremely sensitive to the change in volume, increasing steadily from 0 to 3.46 μ_B as the lattice parameter increases from 3.4 Å (11% volume compression) to 4.1 Å (7% volume expansion).[29] In addition, with the decrease in the lattice constant, the difference in total energy between Γ^{5g} and PM gradually decreases and is almost the same within a small local magnetic moment of Mn atoms, indicating the local magnetic moment could modify the lattice constant and hold the key to spin−lattice coupling. This is consistent with the experimental observation. In particular, the magnetic moment of Mn atoms almost completely originates from Mn 3d electrons from our calculated results, indicating magnetic moments of the Mn 3d electrons play a key role in MVE.

CONCLUSION

In summary, we have revealed a new type of Invar-like material with the Γ^{5g} AFM phase in the $Mn_{3.333}Ni_{0.667}N$ compound. It was found that the fascinating Γ^{5g} AFM phase can be stabilized by the doping of Mn at the Ni site in $Mn_{3+x}Ni_{1-x}N$ compounds. A quantitative relationship between the ordered magnetic moment and lattice variation that controls the ZTE mechanism was provided to investigate the spin−lattice coupling in the Invar-like effect. For this special Γ^{5g} magnetic phase, the MVE was confirmed by the first-principles calculations. We further show that the local magnetic moment of Mn (3d electrons) could modify the lattice constant and hold the key to spin−lattice coupling, which is in agreement with the experimental results. We also suggest that the different contributions (strong or saturation) of MVE cause the diverse ATE (NTE or Invar-like) behaviors observed in various antiperovskite compounds. The results can be readily employed to achieve Invar-like antiperovsikte materials by means of obtaining the pure Γ^{5g} AFM phase of Mn atoms.

ASSOCIATED CONTENT

Supporting Information

Detailed preparation, Rietveld refinement analysis of XRD patterns, additional $M(T)$ curves, and NPD patterns. This material is available free of charge via the Internet at http://pubs.acs.org.

AUTHOR INFORMATION

Corresponding Authors

*E-mail: sunying@buaa.edu.cn.

*E-mail: congwang@buaa.edu.cn.

Notes

The authors declare no competing financial interest.

ACKNOWLEDGMENTS

This work was financially supported by the National Natural Science Foundation of China (NSFC) (51172012 and 51472017) and the Fundamental Research Funds for the Central Universities.

REFERENCES

(1) Salvador, J. R.; Guo, F.; Hogan, T.; Kanatzidis, M. G. *Nature* **2003**, *425*, 702.
(2) Mary, T. A.; Evans, J. S. O.; Vogt, T.; Sleight, A. W. *Science* **1996**, *272*, 90.
(3) Strock, J. D. *Proc. SPIE* **1992**, *1690*, 223.
(4) Grimsey, C. F., Jr. U.S. Patent 3077958, 1963.
(5) Evans, J. S. O.; Hu, Z.; Jorgensen, J. D.; Argyriou, D. N.; Short, S.; Sleight, A. W. *Science* **1997**, *275*, 61.
(6) Gava, V.; Martinotto, A. L.; Perottoni, C. A. *Phys. Rev. Lett.* **2012**, *109*, 195503.
(7) Li, C. W.; Tang, X. L.; Muñoz, J. A.; Keith, J. B.; Tracy, S. J.; Abernathy, D. L.; Fultz, B. *Phys. Rev. Lett.* **2011**, *107*, 195504.
(8) Long, Y. W.; Hayashi, N.; Saito, T.; Azuma, M.; Muranaka, S.; Shimakawa, Y. *Nature* **2009**, *458*, 60.
(9) Azuma, M.; Chen, W. T.; Seki, H.; Czapski, M.; Olga, S.; Oka, K.; Mizumaki, M.; Watanuki, T.; Lshimatsu, N.; Kawamura, N.; Lshiwata, S.; Tucker, M. G.; Shimakawa, Y. C.; Attfield, J. P. *Nat. Commun.* **2011**, *2*, 347.
(10) Chen, J.; Fan, L. L.; Ren, Y.; Pan, Z.; Deng, J. X.; Yu, R. B.; Xing, X. R. *Phys. Rev. Lett.* **2013**, *110*, 115901.
(11) Huang, R. J.; Liu, Y. Y.; Fan, W.; Tan, J.; Xiao, F. R.; Qian, L. H.; Li, L. F. *J. Am. Chem. Soc.* **2013**, *135*, 11469.
(12) Qi, T. F.; Korneta, O. B.; Parkin, S.; De Long, L. E.; Schlottmann, P.; Cao, G. *Phys. Rev. Lett.* **2010**, *105*, 177203.
(13) Schilfgaarde, M. V.; Abrikosov, I. A.; Johansson, B. *Nature* **1999**, *400*, 46.
(14) Kiyama, T.; Yoshimura, K.; Kosuge, K.; Ikeda, Y.; Bando, Y. *Phys. Rev. B* **1996**, *54*, R756.
(15) Taniguchi, T.; Mizusaki, S.; Okada, N.; Nagata, Y.; Mori, K.; Wuernisha, T.; Kamiyama, T.; Hiraoka, N.; Itou, M.; Sakurai, Y.; Ozawa, T. C.; Noro, Y.; Samata, H. *Phys. Rev. B* **2007**, *75*, 024414.
(16) Klimczuk, T.; Walker, H. C.; Springell, R.; Shick, A. B.; Hill, A. H.; Gaczyński, P.; Gofryk, K.; Kimber, S. A. J.; Ritter, C.; Colineau, E.; Griveau, J.-C.; Bouëxière, D.; Eloirdi, R.; Cava, R. J.; Caciuffo, R. *Phys. Rev. B* **2012**, *85*, 174506.
(17) Hicks, T. J.; Pepper, A. R.; Smith, J. H. *J. Phys.: Condens. Matter* **1968**, *1*, 1683.
(18) Uchishiba, H. *J. Phys. Soc. Jpn.* **1971**, *31*, 436.
(19) Yokoyama, T.; Eguchi, K. *Phys. Rev. Lett.* **2013**, *110*, 075901.

DOI: 10.1021/cm504702m
Chem. Mater. 2015, 27, 2495−2501

(20) Wang, C.; Chu, L. H.; Yao, Q. R.; Sun, Y.; Wu, M. M.; Ding, L.; Yan, J.; Na, Y. Y.; Tang, W. H.; Li, G. N.; Huang, Q. Z.; Lynn, J. W. *Phys. Rev. B* **2012**, *85*, 220103(R).
(21) Sun, Y.; Wang, C.; Chu, L. H.; Wen, Y. C.; Nie, M.; Liu, F. S. *Scr. Mater.* **2010**, *62*, 686.
(22) Lin, S.; Wang, B. S.; Lin, J. C.; Huang, Y. N.; Lu, W. J.; Zhao, B. C.; Tong, P.; Song, W. H.; Sun, Y. P. *Appl. Phys. Lett.* **2012**, *101*, 011908.
(23) Huang, R. J.; Li, L. F.; Cai, F. S.; Xu, X. D.; Qian, L. H. *Appl. Phys. Lett.* **2008**, *93*, 081902.
(24) Takenaka, K.; Inagaki, T.; Takagi, H. *Appl. Phys. Lett.* **2009**, *95*, 132508.
(25) Wu, M. M.; Wang, C.; Sun, Y.; Chu, L. H.; Yan, J.; Chen, D. F.; Huang, Q. Z.; Lynn, J. W. *J. Appl. Phys.* **2013**, *114*, 123902.
(26) Takenaka, K.; Ichigo, M.; Hamada, T.; Ozawa, A.; Shibayama, T.; Inagaki, T.; Asano, K. *Sci. Technol. Adv. Mater.* **2014**, *15*, 015009.
(27) Iikubo, S.; Kodama, K.; Takenaka, K.; Takagi, H.; Shamoto, S. *Phys. Rev. B* **2008**, *77*, 020409(R).
(28) Qu, B. Y.; Pan, B. C. *J. Appl. Phys.* **2010**, *108*, 113920.
(29) Lukashev, P.; Sabirianov, R. F.; Belashchenko, K. *Phys. Rev. B* **2008**, *78*, 184414.
(30) Larson, A. C.; Von Dreele, R. B. General Structure Analysis System (GSAS). Technical Report LAUR 86-748; Los Alamos National Laboratory: Los Alamos, NM, 2004.
(31) Fruchart, D.; Bertaut, E. F. *J. Phys. Soc. Jpn.* **1978**, *44*, 781.
(32) Blöchl, P. *Phys. Rev. B* **1994**, *50*, 17953.
(33) Kresse, G.; Joubert, D. *Phys. Rev. B* **1999**, *59*, 1758.
(34) Perdew, J. P.; Burke, K.; Ernzerhof, M. *Phys. Rev. Lett.* **1996**, *77*, 3865.
(35) Sun, Y.; Guo, Y. F.; Tsujimoto, Y.; Yang, J. J.; Shen, B.; Yi, W.; Matsushita, Y.; Wang, C.; Wang, X.; Li, J.; Sathish, C. I.; Yamaura, K. *Inorg. Chem.* **2013**, *52*, 800.
(36) Iikubo, S.; Kodama, K.; Takenaka, K.; Takagi, H.; Takigawa, M.; Shamoto, S. *Phys. Rev. Lett.* **2008**, *101*, 205901.
(37) Takei, W. J.; Heikes, R. R.; Shirane, G. *Phys. Rev.* **1962**, *125*, 6.
(38) Zhang, C. Y.; Zhu, J.; Zhang, M. C.; Zhou, L. J.; Wang, J. *Rengong Jingti Xuebao* **2010**, *39*, 2.
(39) Song, X. Y.; Sun, Z. H.; Huang, Q. Z.; Rettenmayr, M.; Liu, X. M.; Seyring, M.; Li, G. N.; Rao, G. H.; Yin, F. X. *Adv. Mater. (Weinheim, Ger.)* **2011**, *23*, 4690.
(40) Turek, I.; Rusz, J.; Diviš, M. *J. Magn. Magn. Mater.* **2005**, *290*−*291*, 357.

DOI: 10.1021/cm504702m
Chem. Mater. 2015, 27, 2495−2501